Role of stoichiometry and structure in colossal magnetoresistive $La_{1-x}Sr_xMn_{1-y}Ru_yO_{3+\delta}$

Kannan M. Krishnan
Materials Sciences Division, Lawrence Berkeley National Laboratory, University of California, Berkeley, California 94720

H. L. Ju
Materials Sciences Division, Lawrence Berkeley National Laboratory, University of California, Berkeley, California 94720
and Department of Physics, Yonsei University, Seoul 120-749, Korea
(Received 3 December 1998; revised manuscript received 16 July 1999)

We have systematically investigated the effect of stoichiometry [divalent doping (x), controlled oxygen content (δ) by vacuum annealing at elevated temperatures, and substitution (y) of Ru] and structure (substrate induced strain and its relaxation on annealing) on the magnetic/transport properties of the colossal magnetoresistive $La_{1-x}Sr_xMn_{1-y}Ru_yO_{3+\delta}$ bulk and thin films prepared by both sol-gel and pulsed laser deposition techniques. The following results have been found: (1) Oxygen-reduced $La_{0.7}Sr_{0.3}MnO_z$ show a larger resistivity and lower T_c than the corresponding bulk materials. Moreover, their resistivity and MR behavior can be precisely controlled by vacuum annealing and, in fact, they duplicate all the salient features observed in divalent-doped manganites. (2) The metal-insulator transitions of thin films grown on lattice-matched substrates is observed to be a function of thickness due to the accommodation of epitaxial strain and the associated Mn-O-Mn bond-distortions. (3) Ru doped $La_{0.7}Sr_{0.3}Mn_{1-y}Ru_yO_3$, $0 \leqslant y \leqslant 0.2$ samples show a surprisingly small decrease in T_c. This is attributed to the exceptional ability of Ru, unlike other substitutions in Mn sites, to stabilize magnetic ordering at elevated temperatures. (4) Oxygen K-edge (core level excitation of oxygen $1s$ electrons into empty p-like states) electron-energy-loss spectra of divalent-doped $La_{1-x}Sr_xMnO_3$ ($0 < x < 0.7$) and oxygen-reduced $La_{0.7}Sr_{0.3}MnO_z$ thin films conclusively show that these materials are charge-transfer-type insulators with carriers having significant oxygen $2p$ hole character. We discuss the implications of these results on the magnetic and transport properties of manganites and address the implications of our electron-energy-loss spectroscopy measurements on the double exchange mechanism.
[S0163-1829(99)11141-X]

I. INTRODUCTION

Perovskite manganites with the general formula $R_{1-x}A_xMn_{1-y}B_yO_3$ (R=La, Pr, Nd, Sm; A=Ca, Sr, Ba, Pb; B=Fe, Co, Ru) exhibiting large or ''colossal'' magnetoresistance (CMR) (Refs. 1–5) have generated much recent scientific and technological interest. The parent compound, $RMnO_3$ ($Mn^{3+}; t_{2g}^3 e_g^1$) is a magnetic insulator, but $R_{1-x}A_xMnO_3$ transforms into a metallic ferromagnet upon doping in the range $0.2 \leqslant x \leqslant 0.5$.[5,6] $R_{1-x}A_xMnO_3$ exhibits an unusual resistivity peak (T_{MI}) as a function of temperature with metallic and semiconducting behavior below and above the peak, respectively. In well prepared samples, this resistivity peak (T_{MI}) also coincides with the ferromagnetic transition temperature (T_c).[5,7] In some thin films the peak resistivity decreases by several orders of magnitude when an external field of several tesla is applied. For example, the magnetoresistance ratio $\Delta R/R(H)$ (%), defined as $[R(0) - R(H)] \times 100/R(H)$ (%) where $R(0)$ is the resistance in zero field and $R(H)$ is the resistance in an applied field H, is 10^5% in $La_{0.67}Ca_{0.33}Mn_{3-\delta}$ (Ref. 2) and 10^6% in $Nd_{0.7}Sr_{0.3}MnO_{3-\delta}$.[3]

The coexistence of such ferromagnetism and metallic behavior in the manganite perovskites has been traditionally explained within the framework of ''double exchange'' (DE).[8,9] This mechanism is based on a strong exchange interaction between Mn^{3+} and Mn^{4+} ions, while maintaining their spin orientation through intervening filled oxygen $2p$ states. In the simple DE model the transfer integral for an electron is proportional to $\cos(\theta_{ij}/2)$, where θ_{ij} is the angle between the two ionic spins. Thus the DE mechanism qualitatively explains why these manganites become metallic below T_c (well aligned spins) and insulating above T_c (randomly aligned spins), and show large magnetoresistance values due to field induced spin alignment (field induced conductivity, i.e., CMR effect).

Using this elementary DE picture it is clear that stoichiometry (oxygen content, divalent dopant concentration) and associated changes in the valence of the principal constituents of the manganites would play a key role in determining their magnetic and transport properties. Recent theoretical work[9] predicts that DE alone cannot fully explain the resistivity and CMR behavior and in order to do so, the contribution of polarons due to Jahn-Teller distortion effect is proposed. Experimental results such as the giant isotope effect,[10] the sign anomaly of the Hall effect,[11] and Mn-O bond length asymmetry in Mn K-edge extended x-ray-absorption fine structure,[12] further support the polaronic picture of CMR in manganites. Nevertheless, fundamental questions such as the nature of the carriers still remain elusive.

Manganites with the chemical formula $R_{1-x}A_xMn_{1-y}B_yO_3$ have the perovskite structure (Fig. 1) where the A-site atoms (R, A) occupy the center of the cube, the B-site atoms (Mn, B) occupy the corners and the oxygen atoms occupy positions halfway between the B atoms. In general, the size of the A-site atom is too small to stabilize a

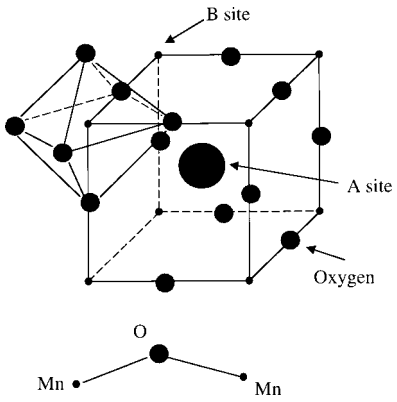

FIG. 1. Crystal structure of $R_{1-x}A_xMn_{1-y}B_yO_3$ (R=La, Pr, Nd, Sm; A=Ca, Sr, Ba, Pb; B=Fe, Co, Ru).

cubic structure; as a result the structure is distorted resulting in an orthorhombic or rhombohedral unit cell. Hence the magnetic and transport properties of manganite perovskites are critically dependent on lattice distortion (Mn-O-Mn angle deviate from 180°) (Ref. 13) which depend on the average size of the cations (A and Ln in $Ln_{1-x}A_xMnO_3$, where A is a divalent dopant and Ln is a lanthanide element), amount of doping[5,7] and oxygen content[14] (i.e., carrier density), and external pressure.[4]

In this paper we have addressed these important issues. The role of stoichiometry is elucidated by vacuum annealing to control oxygen content and by carrying out substitution of Ru for Mn. The fundamental questions on the nature of charge carriers associated with CMR has been addressed based on electron-energy-loss spectroscopy (EELS) measurements of a set of well characterized samples. The role of lattice distortions has been studied using thin films of different thickness where the lattice mismatch due to epitaxial growth on single-crystal substrate is accommodated by uniform strain in the film.

To control the oxygen stoichiometry in a systematic way we have, for the first time, used vacuum annealing methods at temperatures (720–920 K) well below the traditional annealing temperatures (1200–2000 K). It was found that oxygen deficient films show several orders of magnitude larger resistivity values, lower resistivity-peak temperature, smaller saturation moment, lower T_c and enhanced magnetoresistance than those of the corresponding bulk target materials.[2,3,14]

The role of stoichiometry has been further investigated by studying Ru-doped $La_{1-x}A_xMn_{1-y}Ru_yO_3$. La-site ($A$-site) doping studies have been most popularly reported in the perovskite manganites since the doping affects the carrier density and influences the CMR effect. On the other hand, Mn- or B-site doping is rarely performed since B-site doping is believed to be detrimental for the electrical conduction mechanism. It is thought to provide randomness in the electrically active Mn network and break down the DE interactions. In spite of this background, we have found that Ru substitutions on B sites have unusual consequences. Ru has a more delocalized $4d$ orbital than Mn $3d$, Mn is most directly linked with the origin of the CMR phenomena and there is some possibility that Mn may not be the unique DE active element.

Understanding the nature of charge carriers is important for developing a theory of the conduction mechanism in these manganite perovskites. Since $RMnO_3$ is known to be a charge-transfer insulator,[15,16] it contradicts the DE mechanism, which is implicitly based on a Mott-Hubbard type of insulator. We have investigated the origin and nature of charge carriers in these materials which is crucial for a better understanding of the CMR effect. We have found a remarkable correlation between the electrical resistivity and O_{2p} hole density suggesting that the O_{2p} holes are the majority charge carriers in these manganite perovskites.

Finally, the properties of manganite perovskites such as $La_{1-x}Sr_xMnO_3$ (LSMO) are sensitive to internal or external pressure, which affects both the Mn-O bond distance ($d_{\text{Mn-O}}$) and Mn-O-Mn bond angle (ϕ). Slight changes in $d_{\text{Mn-O}}$ or ϕ affect the on-site Coulomb correlation energy and/or bandwidth.[13,17] These changes are to be expected in epitaxially grown LSMO[001]$\|$$LaAlO_3$[001] films which are subjected to compressive strain since d_{LSMO} (3.88 Å) $> d_{\text{LAO}}$ (3.78 Å). We discuss the critical thickness and annealing (strain relaxation) dependence of the transport and structural properties of such thin [001]LSMO/[001]LAO films.

II. EXPERIMENT

Thin films were grown on $LaAlO_3$ substrates by one of two different methods: a polymeric chemical (sol-gel) process or pulsed laser deposition (PLD). The sol-gel process developed in our laboratory[18] used organometallic precursors of lanthanum 2,4-pentanedionate (or Lanthanum acetyl acetonate), manganese (II) acetate and strontium methoxyethoxide which were synthesized from commercially available compounds of Sr metal, manganese acetate hydrate and lanthanum acetyl-acetonate hydrate. 2-methoxyethanol was used as the base solvent. Individual precursors underwent further processing steps of complexation (in required stoichiometric proportions, i.e., La:Sr:Mn:$=1-x:x:1$) and hydrolysis. The solution was spin cast at 2000 rpm for 30 sec on the required substrates to form an amorphous condensed film. Amorphous films were heated at 300 °C on a hot plate, immediately after spin coating, for trapped solvent removal. The minimum thickness obtained for each spin coating was ~500 Å. Multiple deposition/drying cycles were used to make thicker films. A final heat treatment was carried out at 700–1000 °C in air to obtain oxide thin films with the perovskite structure. A key advantage of the sol-gel process is the ability to make films with a wide range of divalent dopant concentration. This is readily accomplished by changing the composition of the precursor solution. For PLD, a 248-nm KrF excimer laser was employed for deposition and was operated with a pulse energy density of 2 J/cm^2 and rate of 1–10 Hz. Typical growth rate was ~0.5–1.0 Å/pulse. During deposition the substrate temperature and oxygen partial pressure were maintained at 600–700 °C and 100–300 mtorr. After the deposition, the films were cooled down to room temperature in an oxygen partial pressure between 200–600 torr. Since uniform growth of thin films with thickness <500 Å is difficult using the sol-gel method, PLD films were used to study the effect of strain in thin films.

The Ru doped manganites, $La_{0.7}Sr_{0.3}Mn_{1-y}Ru_yO_3$ were prepared from stoichiometric mixtures of oxides of La_2O_3, $SrCO_3$, $MnCO_3$, and RuO_2. The samples were reacted at

1100–1200 °C in air with several intermediate grindings until the pure perovskite manganite phase was formed. At the final stage the powders were pelletized and annealed at 1400 °C in air. The $La_{0.7}Sr_{0.3}Mn_{1-y}Ru_yO_3$ films were grown by PLD from these pelletized bulk targets.

Systematic measurements of the role of oxygen stoichiometry on the transport properties of manganites were made using ~200-nm-thick $(001)La_{0.7}Sr_{0.3}MnO_{3-\delta}/(001)LaAlO_3$ films prepared by the sol-gel technique. After the initial deposition process, the films were subsequently annealed in O_2 (1 atm oxygen)/1170 K/1 h to obtain epitaxial oxide thin films with maximum oxygen content (we call these the as-prepared films). Twenty such as-prepared films showing identical resistivity and field response were made. They were subsequently annealed at different temperatures ranging from 720–1020 K for 2 h at a fixed vacuum of 10^{-6} torr. The oxygen content of the films was measured by energy dispersive x-ray spectroscopy (EDXS) using an ultrathin window Si(Li) detector with experimentally measured *k* factors[19] in a transmission electron microscopy (TEM). EDXS results show that the films annealed at 920 K have ~3% less oxygen content than the as-prepared films. For samples of well-defined thickness and using experimentally measured *k* factors, oxygen concentrations can be determined with an accuracy of ~1%. If we normalize the oxygen content of the as-prepared film to 3, that of the 920 K annealed film is ~2.90.

To study the effect of strain on the transport properties, $La_{0.7}Sr_{0.3}MnO_{3-\delta}$ films with thickness ranging from 150–1250 Å, were deposited on $LaAlO_3(001)$ substrates at 640 °C/300 mtorr O_2. These condition were chosen since they give optimal quality of 1000-Å-thick films (low resistivity, high transition temperature, large residual ratio) from a target of composition $La_{0.67}Sr_{0.33}MnO_3$ by pulsed laser deposition. After the deposition the films were cooled down to room temperature at 10 °C/min in an oxygen pressure of 400 torr. Each wafer was cut into two pieces—one half was left as grown and the other half was annealed at 900 °C/1 bar O_2/10 h. The temperature dependence of the dc resistivity in a field H (= 1 T) and zero field was measured using a standard four-probe technique. The field was applied in a direction perpendicular to the film surface and the current direction.

Electron-energy-loss spectroscopy (EELS) data was obtained using a Philips CM200 transmission electron microscope equipped with a field-emission source and a Gatan imaging filter. Spectra were obtained in image mode with a probe convergence angle of 4.0 mrad and energy resolution of the order of 1 eV.

III. RESULTS AND DISCUSSION

A. Doped $La_{1-x}Sr_xMnO_3$ thin films synthesized by sol-gel and PLD methods

Figure 2 illustrates the temperature dependence of the resistivity of the sol-gel derived $La_{1-x}Sr_xMnO_3$ films. Low doped ($x \leq 0.1$) film shows insulating behavior over the entire temperature range. With increasing doping, resistivity decreases—for $x=0.2$ a typical metal-insulator transition is observed at ~260 K; $x=0.3$ shows metallic behavior over the entire temperature range investigated and in addition, has

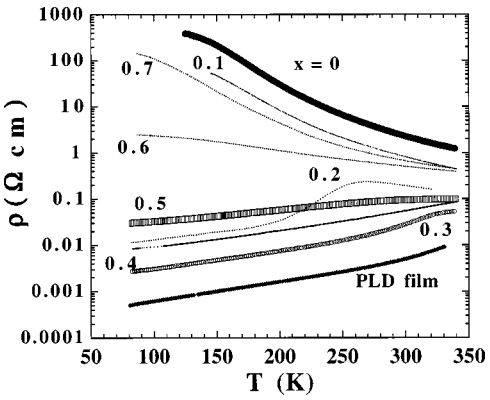

FIG. 2. Temperature dependence of the resistivity of sol-gel derived $La_{1-x}Sr_xMnO_3$ films in the composition range $0 \leq x \leq 0.7$. After the sol-gel process, the $La_{1-x}Sr_xMnO_3$ films were annealed at 700 °C for 1 h in air. EELS data were collected on $x=0$, 0.3, and 0.5 (Fig. 6). Temperature dependence of the resistivity of a $La_{0.67}Sr_{0.33}MnO_3$ film by pulsed laser deposition technique is also shown (bottom curve). The film was annealed at 900 °C for 10 h in 1 atm O_2.

the lowest resistivity among all sol-gel derived LSMO films. The resistivity increases again at higher doping ($x>0.3$). For $x>0.6$, the films show insulating behavior. For these sol-gel derived films, a typical magnetoresistance effect was observed near the ferromagnetic transition temperatures. Figure 2 also shows the temperature dependence of the resistivity of a PLD grown, 100-nm-thick $La_{0.7}Sr_{0.3}MnO_3$ film. The resistivity is clearly more metallic with a sharp increase in resistivity near room temperature corresponding to its high ferromagnetic transition temperature (~370 K). The resistivity value is $\rho_{330\,K} \sim 9\,m\Omega\,cm$ at 330 K, decreases with decreasing temperature and reaches $\rho_{80\,K} \sim 50\,\mu\Omega\,cm$ at $T=80\,K$, which gives a large resistivity ratio $\rho_{330\,K}/\rho_{80\,K}$ of ~18. The resistivity value $\rho_{80\,K} \sim 50\,\mu\Omega\,cm$ is one of the lowest reported for manganite perovskites, indicating a high film quality.

These observations are similar to what is reported in the literature[5] and confirms the viability of the sol-gel synthesis method for high quality thin-film preparation. In addition, divalent doping affects Mn valence but all else is not fixed because oxygen content of the film is not precisely controllable. This is discussed in the next section.

B. Vacuum annealing and controlled oxygen stoichiometry

It is common knowledge that manganite perovskite films grown by PLD show several orders of magnitude larger resistivity values, lower resistivity-peak temperature, smaller saturation moment, lower T_c, enhanced magnetoresistance, and larger lattice parameters when compared with those of the corresponding bulk target materials.[2,3,14] These differences in the magnetotransport properties have been attributed to the differences in the oxygen content[14] even though it has not been systematically controlled to monitor its influence on the CMR phenomenon. To date, to change the oxygen stoichiometry of manganese oxides, only empirical methods such as annealing in N_2 or O_2 at temperatures ranging from 1200–2000 K,[20,21] gettering,[14] and ion implantation[22] have been used. With these methods, precise and reproducible

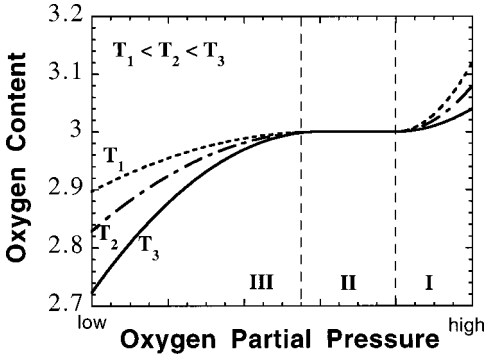

FIG. 3. Schematic diagram of the oxygen content of manganese oxides versus environmental oxygen partial pressure at different temperatures.

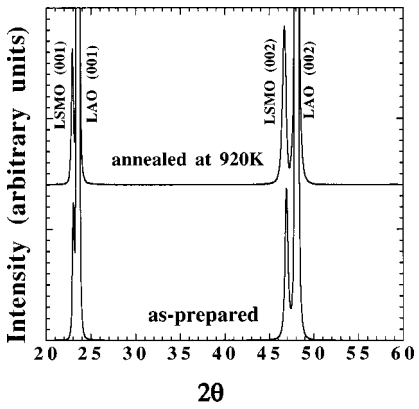

FIG. 4. X-ray-diffraction patterns of films—as-prepared and annealed at 920 K/10^{-6} torr/2 h.

control of oxygen stoichiometry in manganese oxides is difficult. However, the oxygen phase diagram (oxygen content vs ambient oxygen partial pressure) for bulk manganese oxides is partially known[23–25] and this may provide a basis to systematically control the oxygen content and the magnetoresistance (MR) of our manganite thin films. A schematic oxygen phase diagram is shown in Fig. 3. At high ambient oxygen partial pressure (region I: $P_{O_2}/\text{atm} > \sim 10^{-3}$–$10^{-4}$, P_{O_2}: oxygen partial pressure and atm=1 atmospheric pressure), manganites can have oxygen stoichiometry beyond 3, i.e., $3+\delta$. The maximum value of δ (δ_{MAX}) is large for undoped materials; for example, for $LaMnO_{3+\delta}$, $\delta_{MAX} \sim 0.1$.[23] Neutron diffraction, in conjunction with chemical analysis, indicates that $LaMnO_{3+\delta}$ ($\delta > 0$) can also be described with randomly distributed La and Mn vacancies in equal amounts in the stoichiometric perovskite. For doped $La_{1-x}A_xMnO_{3+\delta}$, δ_{MAX} decreases and reaches ~ 0 for $x > 0.3$.[14,23] In addition, for all levels of doping, δ decreases (more stoichiometric) with increasing firing temperature. For example, $LaMnO_{3.12}$ ($\delta = 0.12$), $LaMnO_{3.05}$ ($\delta = 0.05$), $LaMnO_{3.01}$ ($\delta = 0.01$) are obtained when annealed at 1070 K, 1270 K, 1470 K, respectively.[14] At intermediate ambient oxygen partial pressure (region II: $\sim 10^{-6}$–$10^{-8} < P_{O_2}/\text{atm} < \sim 10^{-3}$–$10^{-4}$), manganites tend to be stoichiometric ($\delta = \sim 0$). At low environmental oxygen partial pressure (region III: $\sim 10^{-6}$–$10^{-8} > P_{O_2}/\text{atm}$), the oxygen content of manganites is understoichiometric. Under very low oxygen partial pressures (left end and beyond region III), manganites decompose on annealing. This qualitative phase diagram suggests that systematic control of the oxygen content is possible by annealing in two different ways—either by changing the temperature at a fixed vacuum level or by changing the oxygen partial pressure at a fixed temperature. Here, we report on the control of the oxygen stoichiometry of $La_{0.7}Sr_{0.3}MnO_{3-\delta}$ via fixed-level vacuum annealing at different temperatures and its influence on their resistivity and MR behavior.

The (001) $La_{0.7}Sr_{0.3}MnO_{3-\delta} \| (001)\, LaAlO_3$ films with thickness ~ 200 nm used in this study have been grown by the sol-gel technique.[18] After the sol-gel process, the films were subsequently annealed in O_2 (1 atm oxygen)/1170 K/1 h to obtain epitaxial oxide thin films with maximum oxygen content (we call these the as-prepared films). Twenty such as-prepared films showing identical resistivity and field response were made. They were subsequently annealed at different temperatures for 2 h at a fixed vacuum of 10^{-6} torr ($\sim 3 \times 10^{-10}$ in P_{O_2}/atm: this level of ambient oxygen partial pressure belongs to region III in Fig. 3) to obtain a systematic variation in their oxygen stoichiometry. First, we have annealed the as-grown film at 1170 K and lowered the annealing temperature by 50-K steps. The films annealed at $T > 970$ K show a change in color (from dark yellowish-gray in the as-prepared film to clear gray) and a large room-temperature resistivity $\rho > \sim 10^3\ \Omega$ cm indicating excessive reduction in the oxygen content. Finally, we have been successful in making a series of films with varying resistivity after annealing at 720, 770, 820, and 920 K. The range of annealing temperature used here is well below the conventional annealing temperature, ranging from 1200–2000 K, for the manganites.[14,20] EDXS results show that the films annealed at 920 K have $\sim 3\%$ less oxygen content than the as-prepared films. If we normalize the oxygen content of the as-prepared film to 3, that of 920 K annealed film is ~ 2.90.

The θ–2θ x-ray-diffraction patterns of the two end member films, i.e., as-prepared (the highest oxygen content) and 920 K annealed films (the lowest oxygen content) are shown in Fig. 4. Both films grow with their c axis normal to the substrate plane and are single phase with no other detectable phases or orientations. The 920-K annealed film retains its perovskite structure without any additional peak due to material disintegration. The diffraction peaks are sharp and can be indexed based on the cubic perovskite structure. From the peak positions, we calculate the c-axis lattice constant of the as-grown and 920-K annealed $La_{0.7}Sr_{0.3}MnO_{3-\delta}$ to be 3.87 and 3.89 Å, respectively. It may be interesting to note that the c-axis lattice parameter of $La_{0.7}Sr_{0.3}MnO_{3-\delta}$ film annealed at 920 K is larger than that of the as-grown films. This behavior is similar to that of bulk polycrystalline $La_{0.67}Ba_{0.33}MnO_{3-\delta}$, which also showed an increase in lattice parameter after oxygen stoichiometry reduction.[14] This has been attributed to the increase in average manganese ionic size due to the decrease in average oxidation state upon oxygen reduction. The c-axis lattice parameter of as-prepared films is identical to that of bulk $La_{0.7}Sr_{0.3}MnO_{3-\delta}$ (Ref. 5) which may suggest that the as-prepared films have an oxygen content of ~ 3 ($\delta = \sim 0$).

Figure 5(a) displays the temperature dependence of the resistivity for $H=0$ (filled circle) and $H=1$ T (open circle)

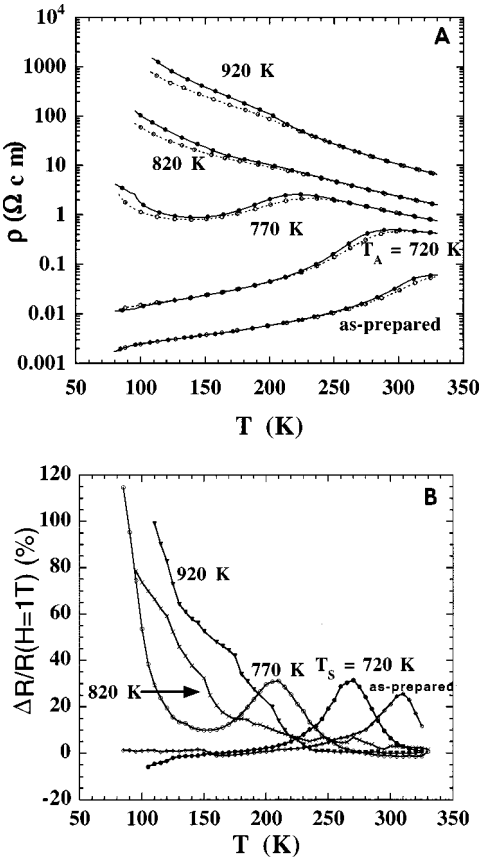

FIG. 5. (a) Temperature dependence of the resistivity taken at $H=0$ (filled circle) and $H=1$ T (empty circle) for as-prepared and vacuum-annealed $La_{0.7}Sr_{0.3}MnO_{3-\delta}$. (b) Temperature dependence of the magnetoresistance ratio $\Delta R/R(H=1\ \mathrm{T})$, (%) for as-prepared and vacuum-annealed $La_{0.7}Sr_{0.3}MnO_{3-\delta}$.

of the as-prepared and vacuum annealed $La_{0.7}Sr_{0.3}MnO_{3-\delta}$ films. The resistivity of $La_{0.7}Sr_{0.3}MnO_{3-\delta}$ increases with increasing annealing temperature (or equivalently with decreasing oxygen content). The as-prepared films show a metallic behavior over the entire temperature range we have investigated. The maximum resistivity ($\sim$60 mΩ cm) was found above room temperature corresponding to its high T_c of $\sim$350 K. The 720 and 770 K annealed films show a resistivity peak at 280 and 210 K, respectively, with metal-like and semiconductorlike behavior below and above the peak. The 770-K annealed film shows a sharp upturn in the resistivity at low temperature. The 820 and 920-K annealed $La_{0.7}Sr_{0.3}MnO_{3-\delta}$ show an insulating behavior over the entire temperature range we have investigated. These features are consistent with a reduction in mobile carrier (Mn^{4+}) density upon decreasing the manganese oxidation state from nominally fully stoichiometric $La_{0.7}Sr_{0.3}MnO_{3-\delta}$ with an average manganese oxidation state $[Mn]=3.3$ for the as-grown films ($\delta=0$) to $[Mn]=3.3-2\delta=\sim 3.10$ for the 920 K annealed films ($\delta=0.1$).

It is interesting to compare our result with bulk data on single crystals of $La_{1-x}Sr_xMnO_3$. Urushibara *et al.*[5] have reported detailed transport studies of doped single-crystalline $La_{1-x}Sr_xMnO_3$. With increasing x (or increasing Mn^{4+} content), the resistivity decreases for $x<\sim 0.3$. The resistivity of single crystals of $La_{1-x}Sr_xMnO_3$ is insulating for $x<0.05$; the resistivity peak appears near T_c and the resistivity shows upturns at low temperature for $x=0.1$ and 0.15. The resistivity shows a metallic behavior for $0.2<x<0.5$. Thus the general resistivity behavior of single-crystalline $La_{1-x}Sr_xMnO_3$ and $La_{0.7}Sr_{0.3}MnO_{3-\delta}$ is quite similar. A significant MR is observed near the resistivity peak for the metallic samples and at low temperatures for the insulating samples. The replotted magnetoresistance ratio $\Delta R/R(H=1\ \mathrm{T})$ for our films, as a function of temperature is shown in Fig. 5(b). The maximum $\Delta R/R(H=1\ \mathrm{T})$ is 26% at 310 K for the as-prepared films and 32% at 270 K for the 720-K annealed films. In addition, the low-temperature MR for these films is small. The 770-K annealed films show a MR peak at 210 K followed by an increase in MR with decreasing temperature, corresponding to the temperature where the resistivity shows upturns. The film also shows a large MR of $\sim$120% at 85 K and 1 T. The 820 and 920 K annealed films show increasing MR with decreasing temperature, similar to their insulating resistivity behavior. In general, with increasing vacuum annealing temperature (or with increasing oxygen deficiency), the MR maximum temperature decreases and the temperature range where MR is significant is lowered, and the maximum MR increases.

The oxygen stoichiometry control via elevated-temperature vacuum annealing can be understood by considering the temperature dependence of the equilibrium constant between ambient oxygen partial pressure and oxygen content. Kuo, Anderson, and Sparlin[25] have studied the oxygen reduction behavior of bulk manganese oxides. They have established a relation between the oxygen content and the ambient oxygen partial pressure for undoped $LaMnO_{3-\delta}$. We assume that their formula is also approximately valid for doped $La_{0.7}Sr_{0.3}MnO_{3-\delta}$ sol-gel derived films. The relation is as follows:

$$K_v=\frac{\delta}{(1-2\delta)^2\cdot(3-\delta)}P_{O_2}^{1/2}, \tag{1}$$

where $K_v=a\exp(-c/T)$ is equilibrium constant, and a and c are positive constants. Equation (1) can be simplified to $K_v=a\exp(-c/T)\approx(\delta/3)P_{O_2}^{1/2}$ if $\delta\ll 1$. Thus K_v is a constant (C) at a fixed temperature, i.e., $K_v\approx(\delta/3)P_{O_2}^{1/2}=C$, and δ is inversely proportional to oxygen partial pressure $P_{O_2}^{1/2}$. Further, as the oxygen partial pressure becomes lower, δ becomes large. Thus by changing vacuum level one can change oxygen content. At fixed vacuum level, K_v is proportional to δ. With increasing temperature K_v increases, thus δ also becomes large. Hence at fixed vacuum level δ increases with increasing temperature.

C. Nature of charge carriers in manganites

Figure 6(a) shows systematic EELS measurements[26–29] of the O_K edge (excitation of O_{1s} electrons into empty p-like states following dipole selection rules) of sol-gel grown $La_{1-x}Sr_xMnO_3$ for $x=0$, 0.3, 0.5 (the temperature dependence of the resistivity data are shown in Fig. 2). O_K edge spectra for the $LaAlO_3$ substrate (which is a perovskite, ionic insulator with completely filled O_{2p} levels) is also shown. In particular, this figure shows the region near the threshold of the O_K edge that is of central interest. The x-ray photoelectron spectroscopy (XPS) binding energy, $E_b=529$ eV (Ref.

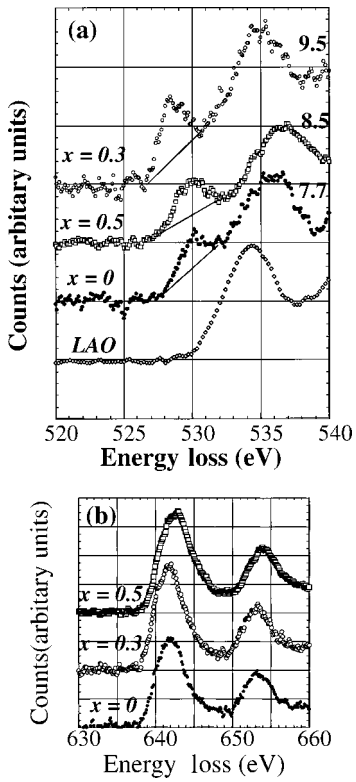

FIG. 6. (a) Oxygen *K*-edge spectra of $La_{1-x}Sr_xMnO_3$ ($x=0$, 0.3, 0.5) and $LaAlO_3$ [the resistivity data are shown in Fig. 2(a)]. The small shifts in the energies of the peaks is due to the drift in the high voltage offsets. (b) Mn $L_{3,2}$-edge spectra of $La_{1-x}Sr_xMnO_3$, which show no discernible change in peak shape or in intensity within the sensitivity of our EELS measurements.

16) which indicates the energy of the O_{1s} level with respect to the Fermi energy is also marked by a narrow band. Any intensity in the vicinity of the Fermi level is a measure of the unoccupied electronic density of states on the oxygen sites. Thus the first feature, the prepeak around 529 eV, is attributed to transitions from O_{1s} to unoccupied states in the O_{2p} band. The relative prepeak intensities have been obtained by normalizing the prepeak intensity above a linear background using the main peak intensity at ~535 eV. The normalized values are 7.7 for $x=0$, 9.5 for $x=0.3$, and 8.5 for $x=0.4$. For $LaAlO_3$ no prepeak is observed and the sharp rise in spectral intensity marking the onset of the edge, ~3 eV above E_F (i.e., at ~532 eV), is attributed to La_{5d} and La_{4f} states hybridized with O_{2p} states.[28] The absence of the prepeak in $LaAlO_3$, an ionic insulator with completely filled O_{2p} states, and its appearance in the $La_{1-x}Sr_xMnO_3$ series is a reflection of the presence of holes on oxygen sites leading to *p*-type conductivity in the latter films. Moreover, the prepeak intensity in $La_{1-x}Sr_xMnO_3$ varies systematically with the conductivity of the films and not with their divalent dopant content. In addition, neither the O_K edge threshold peaks (~532 eV) nor the Mn $L_{3,2}$ (transitions from spin-orbit split $2p_{3/2}$ and $2p_{1/2}$ initial core states to unoccupied $3d$ levels) transitions [Fig. 6(b)] present any discernible change in intensities with divalent doping and/or conductivity of the films. We have also found qualitatively similar correlation between the conductivity and O_{2p} hole intensity for oxygen reduced $La_{0.7}Sr_{0.3}MnO_z$ samples.[29]

Over the range of $La_{1-x}Sr_xMnO_3$ and $La_{0.7}Sr_{0.3}MnO_z$ samples studied, we have observed a significant prepeak at the Fermi level in the O_K edge in EELS, with intensity closely related to the conductivity of the films. The absence of this O_K prepeak in $LaAlO_3$ and its presence in these compounds suggest that the latter are charge-transfer-type oxides.[30] Specifically, doping the parent $LaMnO_3$ with divalent Sr generates unoccupied states in the O_{2p} band and vacuum annealing of $La_{0.7}Sr_{0.3}MnO_z$ which systematically controls the oxygen stoichiometry reduces O_{2p} hole density. Divalent doping or change in oxidation state could also generate Mn^{4+} (Mn holes) but within the sensitivity of our EELS measurements the Mn $L_{3,2}$ transitions show no discernible change in peak shape or in intensity [Fig. 6(b)]. These measurements are in contrast with the conventional DE mechanism where doping is assumed to induce holes on Mn sites (Mn^{4+}) and the interaction between Mn^{3+} and Mn^{4+} drives the ferromagnetic behavior and enhanced conductivity. The O_{2p} hole density, which increases with doping of $LaMnO_3$, has a clear correlation with the magnitude of the resistivity, i.e., the larger the O_{2p} hole density, the smaller the resistivity. This observation implies that the conductivity in these materials is hole driven and that these holes, having predominantly O_{2p} hole character, contribute significantly to the conduction mechanism, including magnetoresistance, in these materials.[29]

D. Unusual substitution effects of Ru on *B* sites

La- or *A*-site doping studies have been most popularly reported in the perovskite manganites since the doping affects carrier density and positively influences the CMR effect. In fact, their properties can be organized along a continuum of cation sizes—the largest cations ($\langle r_A\rangle > 1.24$ Å) exhibit strong CMR whilst the smallest cations ($\langle r_A\rangle < 1.2$ Å) are insulating, charge ordered and do not exhibit ferromagnetism.[31] On the other hand, Mn- or *B*-site doping is rarely performed since it is thought to be detrimental for the electrical conduction mechanism. It randomizes the electrically active Mn network and breaks DE electrons. Despite this background we have attempted to evaluate the effect of Ru in $La_{1-x}A_xMn_{1-y}Ru_yO_3$ for three reasons: Ru has more delocalized $4d$ orbitals than Mn $3d$ orbitals, $SrRuO_3$ is a well known ferromagnet and a highly conducting perovskite and the conductivity in manganites is proportional to its ferromagnetic ordering.

Bulk and thin films of $La_{0.7}Sr_{0.3}Mn_{1-y}Ru_yO_3$ (where $0 \leqslant y \leqslant 0.2$) were prepared by the solid-state reaction method and PLD, respectively. Thin films were grown on $LaAlO_3$ substrates at 300-mTorr oxygen partial pressure and at a substrate temperature of 680 °C. The Ru substituted bulk target of $La_{0.7}Sr_{0.3}Mn_{1-y}Ru_yO_3$ were single phase with orthorhombic symmetry. However, their films grown on (001) $LaAlO_3$ shows cubic symmetry. The (002) peak shows a monotonic increase in lattice parameter from 3.87–3.94 Å with increasing Ru doping. The x-ray pattern (Fig. 7) shows epitaxial growth of Ru-substituted films on the $LaAlO_3$ substrates. Energy dispersive x-ray microanalysis confirmed that the Ru is indeed incorporated into the structure. However, spatially re-

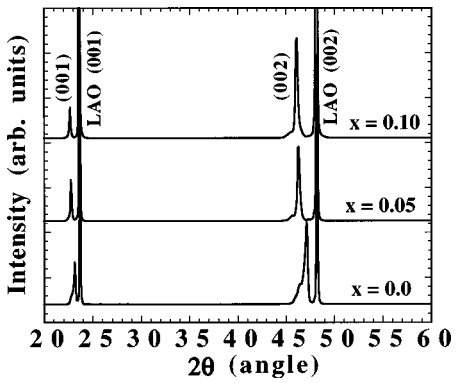

FIG. 7. X-ray diffraction of $La_{0.7}Sr_{0.3}Mn_{1-y}Ru_yO_3$ for $y=0$, 0.05, and 0.1 thin films grown by PLD on $LaAlO_3(100)$ substrates. Note the systematic increase in c parameter (002 reflection) with increasing Ru doping.

solved microanalysis using a 1-nm probe suggests that there is a small segregation of Ru at the grain boundaries.

Magnetization curves for bulk $La_{0.7}Sr_{0.3}Mn_{1-y}Ru_yO_3$ are shown in Fig. 8. The magnetization vs temperature curves indicate a monotonic decrease in T_c, from 365 K for $La_{0.7}Sr_{0.3}MnO_3$ (LSMO) to 335 K for $La_{0.7}Sr_{0.3}Mn_{0.85}Ru_{0.15}O_3$. For $y=0.1$ and 0.15, a shoulder was seen in the M vs T curve. This is possibly due to instrumental error and not due to phase separation since our x-ray results show a single phase material without any impurity phase within the x-ray resolution of about 2%. The Curie temperature for the parent LSMO agrees well with the reported T_c values. Note the unusual doping effect of Ru which shows a very marginal decrease in T_c ($\Delta T_c \sim 35$ K) for doping up to 15% of Ru. A large decrease in T_c in other cases, for example; doping of Al^{3+}, Fe^{3+}, Ti^{4+} has been argued to have a direct effect on the magnetic ordering. The positive influence of Ru doping on magnetic ordering could be interpreted based on the mixed valence states of Ru, as RuO_2, RuO_3, Ru_2O_3, etc. Although similar effects due to variable states has been observed recently by Raveau, Maignan, and Martin[32] on Cr and Co doping in $Pr_{0.5}Ca_{0.5}MnO_3$, it should be noted that Cr and Co ions aid only in the insulator-metal transition and not in the charge-transfer mechanism. However, a rapid disappearance of the magnetic ordering has been observed for Cr and Co doping as small as $y>0.02$. In contrast, Ru substitution up to 15%, sustains magnetic ordering. This can be attributed to the $4d$ metal character of Ru. It is now fairly well understood that the $3d$ electrons are more localized compared to $4d$ electrons. Therefore exchange interaction between Mn-O-Ru could be favored much more than any other transition metals. The presence of variable oxidation state of Ru is evident from the x-ray photoelectron spectrum (Fig. 9) of the Ru substituted bulk samples. The peaks corresponding to 483.0 and 486.2 eV suggests the presence of a possible redox couple involving Ru^{3+}/Ru^{4+} and an interplay of a mixed Zener pair such as $Mn^{3+}/Mn^{4+}-Ru^{3+}/Ru^{4+}$ could be decisive in the charge ordering.

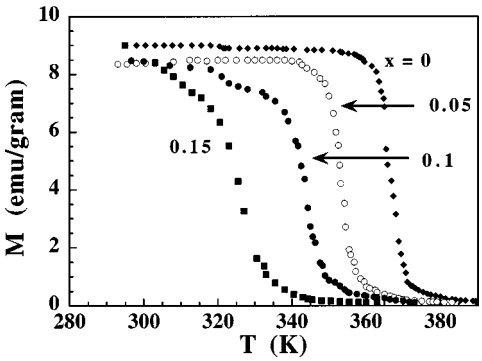

FIG. 8. Temperature dependence of the magnetization (at $H=200$ Oe) of $La_{0.7}Sr_{0.3}Mn_{1-y}Ru_yO_3$ above room temperature in the doping range $0 \leqslant y \leqslant 0.15$.

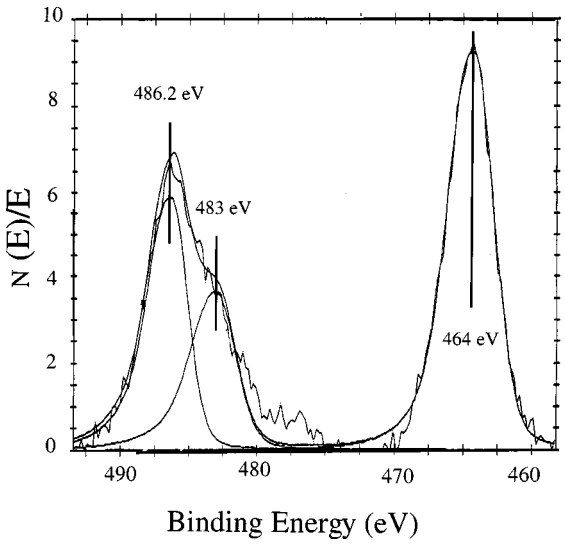

FIG. 9. XPS spectrum showing variable oxidation state for the Ru ($y=0.1$) bulk samples. The peaks corresponding to 483.0 and 486.2 eV suggests the presence of a possible redox couple involving Ru^{3+}/Ru^{4+}.

Figure 10 shows the resistivity versus temperature plot for the parent $La_{0.7}Sr_{0.3}MnO_3$ film and the Ru substituted film $La_{0.7}Sr_{0.3}Mn_{0.9}Ru_{0.1}O_3$. Although ferromagnetic ordering occurs well above the room temperature, resistivity vs temperature plot for the bulk samples show a very broad transition and the metal-insulator transition occurs below 300 K. This is attributed to the role of the grain boundaries. However, upon subsequent annealing at elevated temperatures, well-sintered pellets do show a M-I transition in accordance with the magnetic ordering temperature. As-grown films of $La_{0.7}Sr_{0.3}MnO_3$ and Ru substituted films also show the same semiconducting behavior. In order to overcome this discrepancy, which could occur either from the enhanced role of grain boundaries or from loss of oxygen, the laser targets were sintered with 3% Ag_2O, to promote saturation of oxygen in the films during growth and annealing. It is believed that silver gets oxidized to AgO during laser ablation and during film growth AgO dissociates yielding its oxygen to the $La_{0.7}Sr_{0.3}Mn_{1-y}Ru_yO_3$ films. It is well known that addition of Ag_2O to bulk $YBa_2Cu_3O_7$ and self-doped $La_{1-x}MnO_3$ increases the oxygen content in the $YBa_2Cu_3O_7$ and $La_{0.7}MnO_3$ film, respectively.[33] Consequently, 3% Ag containing LSMO and Ru substituted LSMO films showed a metallic ferromagnetic state below T_c. Further work to un-

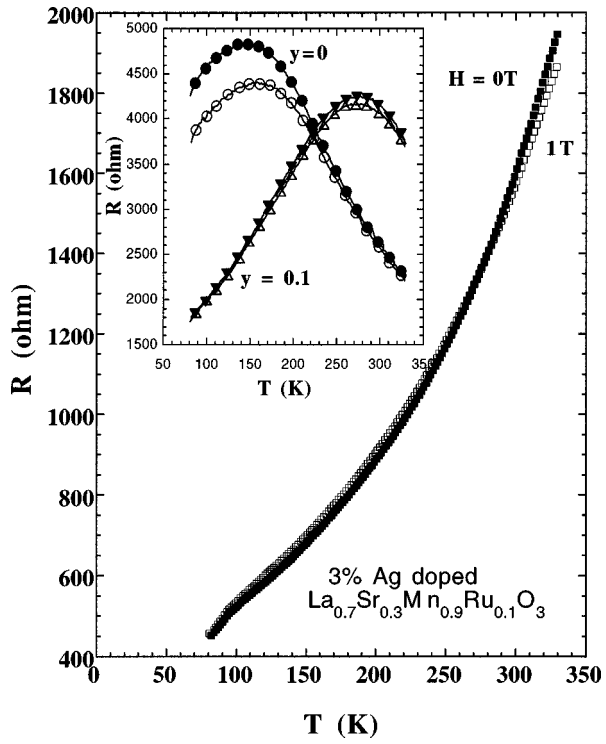

FIG. 10. Temperature dependence of the resistivity at $H=0$ and 1 T of 3% Ag doped $La_{0.7}Sr_{0.3}Mn_{1-y}Ru_yO_3$ ($y=0.1$) film. Inset shows the temperature dependence of the resistivity at $H=0$ and $H=1$ T for parent $y=0$ and $y=0.1$ without Ag doping.

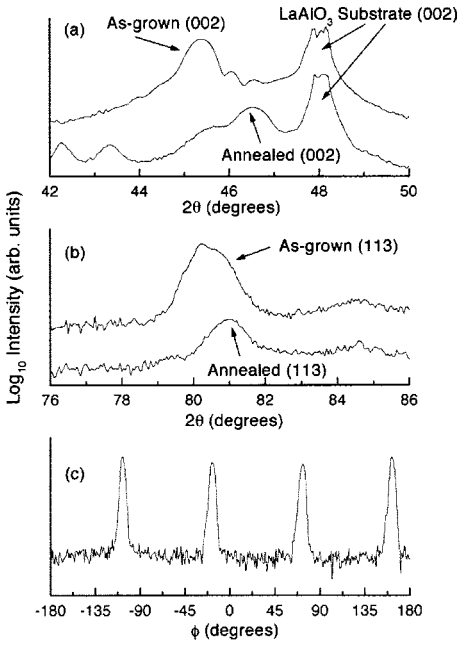

FIG. 11. θ–2θ scans with **q** along the [001] growth direction (a) and the [113] direction (b) for both annealed and as-grown 150-Å-thick samples (top and bottom scans, respectively). The scans from the annealed and as-grown samples were displaced from one another in graphs (a) and (b) for greater clarity. The peaks due to the $LaAlO_3$ substrate, indexed using a pseudoperovskite unit cell, are also indicated. (c) is a Φ scan of the (103) reflection of the annealed sample, which shows a fourfold symmetry characteristic of the pseudoperovskite structure. All samples in this study had the same fourfold symmetry, with the [100] direction coinciding with that of the $LaAlO_3$ substrate.

derstand the unusual substitution behavior of Ru and the role of Ag additions is in progress.

E. The role of lattice strain induced by epitaxy

Properties of thin films, epitaxially grown on lattice-matched substrates, are expected to be different from thick films or bulk because of the large strain effects that have an impact on both the Mn-O bond distance ($d_{\text{Mn-O}}$) and the Mn-O-Mn bond angle (ϕ). Slight changes in $d_{\text{Mn-O}}$ or ϕ affect the on-site Coulomb correlation energy and/or bandwidth and may lead to a metal-insulator transition. Both $d_{\text{Mn-O}}$ and ϕ can be altered either by substitutions,[13,14] external pressure,[4] or, in a controlled fashion, by strain due to epitaxial growth on lattice-matched substrates.[26,34,35] In the latter case, the strain is also a function of the thickness, annealing conditions, and mechanisms of strain relaxation. Although there exist numerous studies of the effect of lattice changes, induced by chemical substitutions and external pressure, on the transport and structure of manganite perovskites, there has been little investigation on the effect of lattice distortion induced by substrate strain on the transport and structure. In addition, the earlier reports were focused on relatively thick films (thickness$\geqslant$1000 Å) most of which were post annealed at high temperature (>900 °C). At these temperatures, a significant lattice relaxation can occur which may make the films unsuitable for studies of the effect of strain on their magnetotransport behavior. Hence we have chosen to study the influence of lattice distortion and strain on the transport properties in the $La_{0.67}Sr_{0.33}MnO_3$ (LSMO) system, which is a metallic and ferromagnetic compound with a high transition temperature of 370 K.[13] Epitaxially grown LSMO[001]$\|$$LaAlO_3$[001] films are expected to be under compressive strain since $d_{\text{LSMO}}(3.88\,\text{Å}) > d_{\text{LAO}}(3.78\,\text{Å})$. We report on the critical thickness and annealing (strain relaxation) dependence of the transport and structural properties of such thin [001]LSMO/[001]LAO films.

$La_{0.7}Sr_{0.3}MnO_{3-\delta}$ films with thickness ranging from 150–1250 Å, were deposited on $LaAlO_3$(001) substrates at 640 °C/300 mtorr O_2. These conditions were chosen since it gives optimal quality of 1000-Å thick films (low resistivity, high transition temperature, large residual ratio) synthesized form a target of composition $La_{0.67}Sr_{0.63}MnO_3$ by pulsed laser deposition. After the deposition the films were cooled down to room temperature at 10 °C min in an oxygen pressure of 400 torr. Each wafer was cut into two pieces—one half was left as grown and the other half was annealed at 900 °C/1 bar O_2/10 h.

Figure 11 shows representative x-ray data from both annealed and as-grown 150-Å-thick samples. Similar results were obtained from the 700 and 1250-Å samples, although the peaks in the thicker samples were generally narrower and more intense. The data in Fig. 11(a) was obtained with the scattering vector **q** along the [001] direction, so that the sample peaks correspond to the (002) reflection. In both of these scans, the peak near $2\theta=48°$ is a substrate peak. The top scan, measured in the as-grown sample, shows a single

TABLE I. Lattice parameters of $La_{0.67}Sr_{0.33}MnO_3/LaAlO_3$ thin-film samples determined from x-ray-diffraction data. The *c* axis represents the lattice parameter along the growth [001] direction, while the *a* axis represents the [010] and [100] directions. The corresponding Mn-O-Mn bond angles (ϕ) and the Mn-O bond distances, both in-plane and out of plane, are also shown.

Sample	c (Å)	a (Å)	d_{out} (Å)	ϕ_{out}	d_{in} (Å)	ϕ_{in}
150-Å as-grown	3.99	3.82	2.00	180°	1.96	151°
150-Å annealed	3.91	3.87	1.96	171°	1.96	160°
700-Å as-grown	3.98	3.85	1.99	180°	1.96	156°
700-Å annealed	3.90	3.88	1.95	167°	1.96	162°
1250-Å as-grown	3.91	3.82	1.96	171°	1.96	151°
1250-Å annealed	3.88	3.87	1.96	162°	1.96	160°
bulk	3.88	3.88	1.96	162°	1.96	162°

peak at approximately $2\theta = 45.5°$, while in the other, smaller peaks result from the finite thickness of the film. The bottom scan in (a), obtained from the annealed sample, shows several peaks, the strongest of which appears near $2\theta = 46.5°$. The other weaker peaks could be due to different phases formed during the annealing process. Clearly, the effect of annealing is to shift the peaks to higher angles, which means that the (001) interplanar distance contracts. The scans in Fig. 11(b) were obtained with **q** along the [113] direction. The top scan again represents the as-grown sample, while the bottom scan represents the annealed sample. The effect of annealing in this case is to shift the peak to higher angles. Figure 11(c) is a Φ scan of the (103) reflection of the annealed 150-Å-thick sample, showing the fourfold symmetry characteristic of the tetragonal crystal structure. All samples showed the same fourfold symmetry. From scans such as those shown in Figs. 11(a) and 11(b), the in-plane and out-of-plane lattice parameters were calculated assuming that the [100] and [010] in-plane directions are equivalent, and that the unit cell is tetragonal. Similar scans of the (103) reflection were used to confirm the results. The results are shown in Table I. It is clear that annealing causes the *c* axis (along the growth direction) to contract while the *a* axis (in the plane) expands.

The temperature dependence of the resistivity for the as-grown and annealed films is shown in Fig. 12. The resistivity of the as-grown films [Fig. 12(a)] shows a critical dependence on thickness (t). For $t = 150$ Å, it is completely insulating over the entire temperature range investigated with a significant magnetoresistance (MR) effect observed below 200 K. MR increases with a decrease in temperature and reaches ~50% at 1 T and 80 K. However, the absolute magnitude of the resistivity at 80 K is ~1000 mΩ cm (or ~1 Ω cm) and rather small compared to that of insulating bulk samples ($>10^3$ Ω cm).[10] For $t = 700$ Å, the zero-field resistivity is also insulating (with the magnitude of the resistivity smaller than that for $t = 150$ Å), but when a field of 1 T is applied the resistivity, $\rho_{H=1\,T}(T)$ is suppressed below 270 K and shows a peak around 180 K, with metal-like behavior at lower temperatures. The MR for $t = 700$ Å was found to increase with decreasing temperature. Unlike the above two cases, for $t = 1250$ Å a metallic behavior with a room temperature resistivity of ~2 mΩ cm, along with a large MR effect near and above room temperature but with insignificant MR at low temperature, is observed.

Contrary to the critical thickness dependence of resistivity and MR for the as-grown films, the annealed films [Fig. 12(b)] uniformly show a metallic behavior with significant MR above room temperature. However, the magnitude of the resistivity decreases with an increase in film thickness. For example, the resistivity at 330 K, $\rho_{330\,K}$ is 2.7 mΩ cm for 150 Å, 1.6 mΩ cm for 700 Å, 1.2 mΩ cm for 1250 Å. The resistivity ratio $\rho_{330\,K}/\rho_{80\,K}$ increases with increasing film thickness—$\rho_{330\,K}/\rho_{80\,K} = \sim 6$, ~8, ~12 for 150, 700, and 1250-Å-thick films, respectively. Moreover, the thicker the

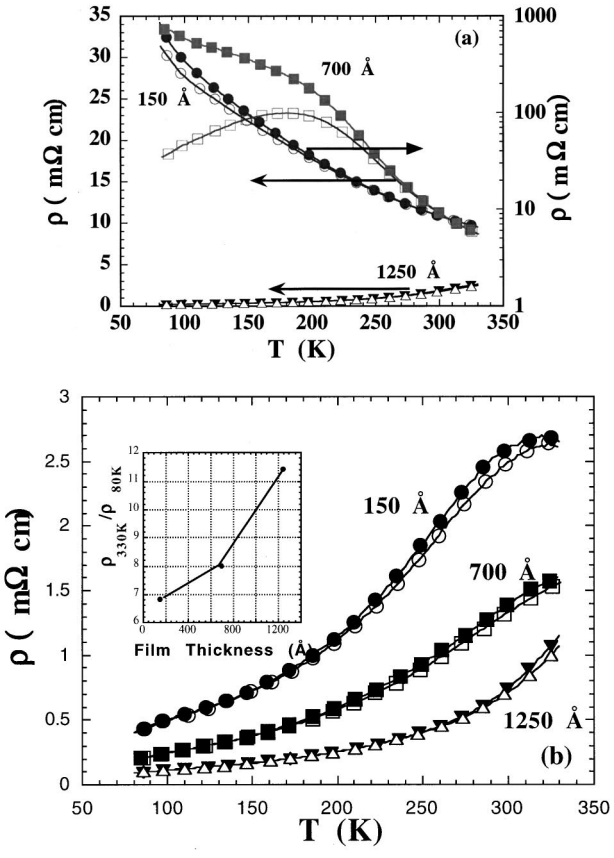

FIG. 12. Temperature dependence of the resistivity of $La_{0.67}Sr_{0.33}MnO_3$ films with thicknesses of 150, 700, and 1250 Å. Both as-grown (a) and annealed films (b) without field (full symbol) and with an applied field of 1 T (empty symbol) are shown. Inset shows the resistivity ratio $\rho_{330\,K}/\rho_{80\,K}$ ($\rho_{330\,K}$: the resistivity at 330 K, $\rho_{80\,K}$: the resistivity at 80 K).

film the higher the resistivity peak temperature. The temperature dependence of resistivity reveals that the 150-Å-thick film exhibits a resistivity peak at 320 K, 700-Å-thick film exhibits a resistivity approaching a peak, and the 1250-Å-thick film exhibits resistivity with a sharp increase.

Changes in lattice constants of perovskites determine two key structural parameters that impact on their transport properties: Mn-O-Mn bond angle (ϕ) and bond distance ($d_{\text{Mn-O}}$) (note: both in-plane and out-of-plane values are shown in Table I). However, it has been shown that for $R_{0.67}A_{0.33}MnO_3$ (R=La, Pr, Nd, Y: A=Ca, Sr, Ba), changes in (R, A)-site ionic size only affect ϕ, with $d_{\text{Mn-O}}$ remaining unchanged ($d_{\text{Mn-O}}=1.96$ Å).[36] This corresponds to a maximum lattice parameter of 3.92 Å. Hence it is reasonable to assume that larger values of the lattice parameter imply stretching of $d_{\text{Mn-O}}$ (ϕ fixed at 180°) and smaller lattice parameters imply a contraction of ϕ ($d_{\text{Mn-O}}$ fixed at 1.96 Å). In the as-grown films, a is ~3.82–3.85 Å but c depends on film thickness, i.e., $c=3.99$ Å for $t=150$ Å and $c=3.91$ Å for $t=1250$ Å. Thus the thickness dependence of the resistivity as a function of temperature of as-grown LSMO thin films may be related to changes in the c parameter. For bulk $La_{0.67}Sr_{0.33}MnO_3$, where $d_{\text{Mn-O}}=1.96$ Å and $a=c=3.88$ Å,[13] ϕ is found to be ~162°. For tetragonally distorted LSMO thin films ϕ and $d_{\text{Mn-O}}$ are, in principle, different along the a- (in-plane) and c- (out of plane) axis directions. For the as-grown films, the in-plane Mn-O-Mn bond angle, ϕ_{in} is ~151–156° and this decrease in the bond angle (with respect to the bulk) may significantly reduce the double exchange interaction. However, ϕ_{in} and d_{in} are independent of thickness and may not explain the thickness dependence of the resistivity. On the other hand, the out-of-plane Mn-O-Mn angle, ϕ_{out} for the as-grown films is ~180° and the out-of-plane Mn-O distance, d_{out} is significantly stretched (Table I). d_{out} for the insulating, $t=150$ Å, as-grown film is greater than that for metallic $t=1250$-Å film by 0.04 Å. The influence of the bond distance $d_{\text{Ti-O}}$ (distance between Ti and O) on the transport properties has been reported[36] for the bulk, cubic perovskite ($\phi=180°$ between Ti-O-Ti) compound $Nd_{1-x}Ba_xTiO_3$ (NBTO) where a small increase in $d_{\text{Ti-O}}$ (~0.02 Å) is responsible for a change from metallic to insulating behavior for $0.7\leqslant x\leqslant 0.9$. The change in $d_{\text{Mn-O}}$ in LSMO thin films, particularly in the out-of-plane direction, is greater than the change in $d_{\text{Ti-O}}$ of NBTO and may be responsible for its insulating behavior. However, there are important differences in the electronic transport between LSMO and NBTO. While the conduction pathway in bulk NBTO is three dimensional, in LSMO thin films the conduction pathway is quasi-two-dimensional. It is also known that the bandwidth of cubic perovskite materials is proportional to $1/(d_{\text{Mn-O}})^3$.[37] Thus the larger the value of $d_{\text{Mn-O}}$, the smaller the bandwidth. In addition to a decrease in the bandwidth, an increase in $d_{\text{Mn-O}}$ results in an increase in the Hubbard correlation energy. From the data we may conclude that the electronic transport along the c direction is important in the current flow. As a first approximation, the charge carriers in thin LSMO films move with Brownian motion and hence the larger the out-of-plane lattice parameter, the smaller the electrical conduction along c. Thus the difference in c for the as-grown films may be responsible for the critical dependence of the resistivity on the film thickness for as-grown films. For all films, after annealing, the c axis contracts and the a axis expands resulting in a cubic structure with $a=c\sim 3.88$ Å. There is neither change in a, c, nor the temperature dependence of the resistivity as a function of thickness. The minor differences, i.e., the magnitude of the resistivity and ratio $\rho_{300\text{ K}}/\rho_{80\text{ K}}$, may be due to variations in the dislocation network created to accommodate the coherency strain.

IV. CONCLUSION

Using the approximately known oxygen phase diagram, we have successfully controlled the oxygen stoichiometry, the resistivity, and magnetoresistive behavior of sol-gel derived $La_{0.7}Sr_{0.3}MnO_{3-\delta}$ films. Vacuum annealed films at temperatures ranging from 720–920 K show increasing magnetoresistance with a decrease of oxygen stoichiometry, varied resistivity from metallic to insulating and interesting magnetoresistance behavior. This work shows that precise and reproducible control of oxygen stoichiometry, resistivity and MR behavior is possible without changing the divalent dopant concentration.

The resistivity of as-grown/annealed $(001)La_{0.67}Sr_{0.33}MnO_3/(001)LaAlO_3(001)$ epitaxial thin films is critically dependent on their thickness due to the compressive strain induced by lattice matching to the $LaAlO_3$ substrate. The thinner the films, the more the strain. As a result, thinner films show severe lattice distortions and higher resistivity values. The 150-Å-thick films show insulating behavior, 700-Å-thick films show metal-insulator transitions, and 1250-Å-thick films show metallic behavior. After annealing, the lattice strain is relieved and all the annealed films show identical metallic behavior, similarly to thick films or corresponding bulk materials.

Using EELS we have observed a prepeak in the oxygen K edge, corresponding to transitions to empty states in the O_{2p} band at the Fermi level. This prepeak intensity systematically increases with an increase in conductivity, through divalent doping or variation in oxygen stoichiometry. This confirms that these manganite perovskite thin films are charge-transfer-type oxides with carriers having significant oxygen $2p$ hole character. Based on these results, we argued that in addition to lattice distortion effects the double exchange mechanism has to include the role of oxygen hole density to provide a satisfactory description of their transport properties.[38]

The magnetic and transport properties of manganite perovskites are sensitive to doping, oxygen stoichiometry, lattice distortion by substrate strain, and lattice relaxation. The Ru doped $La_{0.7}Sr_{0.3}Mn_{1-y}Ru_yO_3$ maintains a relatively high transition temperature. The decrease in T_c at a doping level of $y=0.15$ is only ~30 K which is considerably smaller than the one observed for doping with other elements such as Fe ($\Delta T_c=\sim 100$ K). It is postulated that this small decrease in T_c is due to the delocalized nature of $4d$ orbital in Ru.

ACKNOWLEDGMENTS

We thank A. R. Modak for the preparation of the stock solution of $La_{1-x}Sr_xMnO_z$, C. Nelson for assistance with

the newly installed Phillips CM200/FEG instrument, and E. J. Echer for the measurement of the oxygen content by EDXS at the National Center for Electron Microscopy, Dr. J. B. Torrance and Dr. S. Sundar Manoharan for helpful discussions, Dr. Frank Ogeltree for recording the XPS data, Dr. D. Lederman for x-ray data, and Greg Kusinski for a critical reading of the manuscript. This work was supported by the Director, Office of Energy Research, Office of Basic Energy Sciences, Materials Sciences Division of the U.S. Department of Energy under Contract No. DE-AC03-76SF00098.

[1] R. von Helmolt, J. Wecker, B. Holzapfel, L. Schultz, and K. Samwer, Phys. Rev. Lett. **71**, 2331 (1993); K. Chahara, T. Ohno, M. Kasai, and Y. Kozono, Appl. Phys. Lett. **63**, 1990 (1993).

[2] S. Jin, T. H. Tiefel, M. McCormack, R. A. Fastnacht, R. Ramesh, and L. H. Chen, Science **264**, 413 (1994).

[3] G. C. Xiong, Qi Li, H. L. Ju, S. N. Mao, L. Senapati, X. X. Xi, R. L. Greene, and T. Venkatesan, Appl. Phys. Lett. **66**, 1427 (1995).

[4] K. Khazeni, Y. X. Jia, Li Lu, Vincent H. Crespi, Marvin L. Cohen, and A. Zettl, Phys. Rev. Lett. **76**, 295 (1996).

[5] A. Urushibara, Y. Moritomo, T. Arima, G. Kito, and Y. Tokura, Phys. Rev. B **51**, 14 103 (1995).

[6] G. H. Jonker and J. H. Van Santen, Physica (Utrecht) **16**, 337 (1950).

[7] H. L. Ju, C. Kwon, Qi Li, R. L. Greene, and T. Venkatesan, Appl. Phys. Lett. **65**, 2108 (1994).

[8] P. G. de Gennes, Phys. Rev. **118**, 141 (1960).

[9] A. J. Millis, P. B. Little Wood, and B. I. Shraiman, Phys. Rev. Lett. **74**, 5144 (1995).

[10] J.-S. Zhou and J. B. Goodenough, Phys. Rev. Lett. **80**, 2665 (1998).

[11] M. Jaime, Phys. Rev. Lett. **78**, 951 (1997).

[12] L. Lanzara, N. L. Saini, M. Brunelli, F. Natali, A. Bianconi, P. G. Radaelli, and S.-W. Cheong, Phys. Rev. Lett. **81**, 878 (1998).

[13] H. Y. Hwang, S.-W. Cheong, P. G. Radaelli, M. Marezio, and B. Batlogg, Phys. Rev. Lett. **75**, 914 (1995).

[14] H. L. Ju, J. Gopalakrishnan, J. L. Peng, Qi Li, G. C. Xiong, T. Venkatesan, and R. L. Greene, Phys. Rev. B **51**, 6143 (1995).

[15] J. B. Torrance, Physica C **182**, 351 (1991).

[16] T. Saitoh, A. E. Bocquet, T. Mizokawa, H. Namatame, A. Fujimori, M. Abbate, Y. Takeda, and M. Takano, Phys. Rev. B **51**, 13 942 (1995).

[17] J. B. Torrance, P. Lacorre, A. I. Nazzal, E. J. Ansaldo, and C. Niedermayer, Phys. Rev. B **45**, 8209 (1992).

[18] Kannan M. Krishnan, A. R. Modak, H. L. Ju, and P. Bandaru, in *Ceramic Microstructures: Control at the Atomic Level*, edited by A. P. Tomsia and A. M. Glaeser (Plenum, New York, 1998), p. 597.

[19] Kannan M. Krishnan and C. J. Echer, *Analytical Electron Microscopy*, edited by D. C. Joy (San Fransisco Press, San Francisco, 1987).

[20] A. Gupta, T. R. MaGuire, P. R. Duncombe, M. Rupp, J. Z. Sun, W. J. Gallagher, and Gang Xiao, Appl. Phys. Lett. **67**, 3494 (1995).

[21] M. F. Hundley, M. Hawley, R. H. Heffner, Q. X. Jia, J. J. Neumeier, J. Tesmer, J. D. Thompson, and X. D. Wu, Appl. Phys. Lett. **67**, 860 (1995).

[22] C. H. Chen, V. Talyansky, C. Kwon, M. Rajeswari, R. P. Sharma, R. Ramesh, T. Venkatesan, J. Melngailis, Z. Zhang, and W. K. Chu, Appl. Phys. Lett. **69**, 3089 (1996).

[23] Y. Takeda, S. Nakai, T. Kojima, R. Kanno, N. Imannshii, G. Q. Shen, O. Yamamoto, M. Mori, C. Asakawa, and T. Abe, Mater. Res. Bull. **26**, 132 (1991).

[24] J. A. M. van Roosmalen and E. H. P. Cordfunke, J. Solid State Chem. **110**, 100 (1994).

[25] J. H. Kuo, H. U. Anderson, and D. M. Sparlin, J. Solid State Chem. **83**, 52 (1989).

[26] R. F. Egerton, *EELS in the Electron Microscope* (Plenum, New York, 1986).

[27] Established techniques for the determination of the electronic structure of such materials, such as x-ray photoelectron (XPS) and x-ray-absorption (XAS) spectroscopies, are only surface sensitive with probing depths of 10–50 Å. To be effective, these techniques require that the surfaces prepared have electronic structures representative of the bulk. This is particularly difficult to achieve for these perovskite manganites since their surfaces are chemically unstable (Ref. 16) and transform with the evolution of oxygen under vacuum conditions.

[28] N. Nücker, J. Fink, J. C. Fuggle, P. J. Durham, and W. M. Temmerman, Phys. Rev. B **37**, 5158 (1988).

[29] H. L. Ju, H.-C. Sohn, and K. M. Krishnan, Phys. Rev. Lett. **79**, 3230 (1997).

[30] G. A. Zaanen, G. A. Sawatzky, and J. W. Allen, Phys. Rev. Lett. **55**, 418 (1985).

[31] C. N. R. Rao and A. K. Cheetham, Science **276**, 911 (1997).

[32] B. Raveau, A. Maignan, and C. Martin, J. Solid State Chem. **130**, 162 (1997).

[33] D. Kumar, K. M. Satylakshmi, S. S. Manoharan, and M. S. Hegde, Bull. Mater. Sci. **17** (6), 625 (1994).

[34] S. Jin, T. H. Tiefel, M. McCormack, H. M. O'Bryan, L. H. Chen, R. Ramesh, and D. Schurig, Appl. Phys. Lett. **67**, 557 (1995).

[35] J. L. García-Muñoz, J. Fontcuberta, B. Martínez, A. Seffar, S. Piñol, and X. Obradors, Phys. Rev. B **55**, R668 (1997).

[36] C. Eylem, H. L. Ju, B. W. Eichhorn, and R. L. Greene, J. Solid State Chem. **114**, 164 (1995).

[37] T. Y. Koo, S. H. Park, K.-B. Lee, and Y. H. Jeong, Appl. Phys. Lett. **71**, 977 (1997).

[38] Recently, a doped-polaronic semiconductor model, which is largely based on our measurements, has been developed for the origin of the colossal magnetoresistive oxides: A. S. Alexandrov and A. M. Bratkovsky, Phys. Rev. Lett. **82**, 141 (1999).